INTERNATIONAL JOURNAL OF
NUMERICAL ANALYSIS AND MODELING
Volume 17, Number 5, Pages 679–694

LOCALLY CONSERVATIVE FINITE ELEMENT SOLUTIONS FOR PARABOLIC EQUATIONS

WENBO GONG AND QINGSONG ZOU

Abstract. In this paper, we post-process the finite element solutions for parabolic equations to meet discrete conservation laws in element-level. The post-processing procedure are implemented by two different approaches : one is by computing a globally continuous flux function and the other is by computing the so-called finite-volume-element-like solution. Both approaches only require to solve a small linear system on each element of the underlying mesh. The post-processed flux converges to the exact flux with optimal convergence rates. Numerical computations verify our theoretical findings.

Key words. Conservation laws, postprocessing, finite volume solution.

1. Introduction.

We consider numerical solutions of the following spatially-two-dimensional parabolic equations :

$$\begin{cases} u_t - \nabla \cdot (\kappa(\mathbf{x})\nabla u) = f(\mathbf{x},t), \quad (\mathbf{x},t) \in \Omega \times (0,T], \\ u = 0, \quad \mathbf{x} \in \partial\Omega \times (0,T], \\ u(\mathbf{x},0) = u_0(\mathbf{x}), \quad \mathbf{x} \in \Omega, \end{cases} \tag{1}$$

where Ω is a convex bounded polygonal domain in $\mathbb{R}^2$ with boundary $\partial\Omega$. We assume that $f(\mathbf{x},t) \in L^2(\Omega)$ for $t \in [0,T]$ and the coefficient function κ is Lipschitz continuous, there exits two positive constants κ_* and κ^* such that $\kappa_* \leqslant \kappa(\mathbf{x}) \leqslant \kappa^*$ for almost all $\mathbf{x} \in \Omega$. The above parabolic equations are widely used in the modelling of physical phenomena such as that from hydrological, biological and biogeochemical disciplines [6, 10, 19, 30]. Due to the lack of analytical solution and the expensive cost of physical experiments, numerical simulations received a great deal of attention in the study of parabolic problems. Among all numerical methods, those who guarantee locally conservation laws received a great deal of attention.

The finite volume method (FVM, see e.g.,[3, 11, 13, 17, 16])) is an important numerical method which preserves the conservation law in element level, it is very popular in computational fluid dynamics(CFD, see e.g., [24]). However, the linear algebraic system resulting from the FVM is generally non-symmetric, its implementation and analysis is challenging, especially for high order schemes(c.f., [2, 12, 18, 25, 26, 29]). The linear system derived from the finite element method(FEM) is symmetric and thus can be computed with many fast solvers. The FEM solutions, however, do not satisfy the local conservation laws. Therefore, many efforts have been made to post-process FEM solutions to derive solutions which satisfy local conservation laws during the past several decades. To the best of our knowledge, the first work on post-processing of the FEM solutions to derive locally conservative fluxes can be traced back to Douglas, Dupont and Wheeler([9]), which is designed in 1974 for elliptic equations. Thereafter a lot of works along this direction are reported in the literature. For instances, in 2006, Bochev and Gunzburger

Received by the editors January 15, 2020 and, in revised form, May 19, 2020.
2000 *Mathematics Subject Classification.* 35R35, 49J40, 60G40.

develop a flux-correction procedure for the Darcy flow equation based on the least-squares method, their derived solution guarantees local conservation law without compromising its L^2 accuracy ([5]). In 2007, Cockburn et al. present a two-step post-processing algorithm to generate a conservative flux([8]). In 2013, Pouliot et al. post-process the FEM solutions based on the flux superconvergent-points([21]). In [28] , Zhang et al. develop elemenwisely conservative flux by correcting the FEM solution element-by-element. In [32], Zou et al. derive volume-wisely conservative flux by solving a small linear system in each element of the underlying mesh.

In the present paper, we apply the post-processing techniques in [32] to parabolic equations. As that in [32], our post procedure here can be implemented element-wisely. Moreover, our post processing techniques share almost all advantages possessed by the techniques in [32]. For instances, the post-precessed numerical flux satisfies the local conservation law and converges to the exact flux with optimal orders, etc. However, since the parabolic equation is related to the time evolution, our post-processing procedure here is significantly different from that for elliptic equations by solving an ordinary differential equation system in each element of the underlying mesh instead of solving a static linear system in each element of the underlying mesh which is done in [32].

The rest of the paper is organized as below. In Section 2, we present semi-discrete FEM and FVM solutions and their related properties. In Section 3, we post-process the semi-discrete FEM solution to obtain a globally continuous flux function and a finite-volume-element-like solution, both locally conservative. The approximation property of the post-processed solution will be also discussed. In Section 4, we illustrate how to implement our post-processing techniques in practical algorithms associated with a certain temporal discretization. In Section 5, several numerical experiments are made to demonstrate the efficiency and accuracy of our post-processing algorithms.

We close the section by an introduction of some notation. Let $D \subset \mathbb{R}^2$ be an open bounded domain with Lipschitz continuous boundary. We adopt standard notations for Sobolev spaces such as $W^{m,p}(D)$ on sub-domain $D \subset \Omega$ equipped with the norm $\|\cdot\|_{m,p,D}$ and semi-norm $|\cdot|_{m,p,D}$. When $D = \Omega$, we omit the index D; and if $p = 2$, we set $W^{m,p}(D) = H^m(D)$, $\|\cdot\|_{m,p,D} = \|\cdot\|_{m,D}$, and $|\cdot|_{m,p,D} = |\cdot|_{m,D}$. Notation $A \lesssim B$ implies that A can be bounded by B multiplied by a constant independent of the mesh size h. $A \simeq B$ means that both $A \lesssim B$ and $B \lesssim A$.

2. Semi-discrete finite element and finite volume solutions.

To illustrate our basic idea on post-processing, we only present the semi-discrete schemes instead of fully-discrete schemes for (1) in this section. We begin our presentation with an introduction on the spatial discretization. Let $\mathcal{T}_h = \{\tau\}$ be a family of quasi-uniform and shape-regular *triangulation* on Ω. We denote by $\mathcal{N}_h$, $\mathring{\mathcal{N}}_h$, $\mathcal{E}_h$, $\mathring{\mathcal{E}}_h$ the set of all vertices, the set of internal vertices, the set of all edges, and the set of internal edges, respectively. Let the standard linear finite element space be

$$V_h = \{v \in C(\overline{\Omega}) : v|_\tau \in \mathcal{P}_1, \forall \tau \in \mathcal{T}_h, v|_{\partial\Omega} = 0\},$$

where $\mathcal{P}_1$ is the space of all first-order polynomials. It's known that $V_h \subset H_0^1(\Omega)$ and it has a standard Lagrange basis $S_h(T) = span\{\phi_P, P \in \mathring{\mathcal{N}}_h\}$, where $\phi_P \in V_h$ is nodal basis function satisfying $\phi_P(P') = \delta_{PP'}$.

The semi-discrete finite element method for (1) is to find a function $u_h(\cdot,t) \in V_h, t \in [0,T]$, such that

$$\begin{cases} (u_{h,t}(\cdot,t), v_h) + a(u_h(\cdot,t), v_h) = (f(\cdot,t), v_h), \quad \forall v_h \in V_h, \\ u_h(\mathbf{x},0) = u_{0h}(\mathbf{x}), \quad \mathbf{x} \in \Omega, \end{cases} \tag{2}$$

where for all $v, w \in H^1(\Omega)$

$$a(v,w) = \int_\Omega \kappa \nabla v \cdot \nabla w d\boldsymbol{x}, \qquad (v,w) = \int_\Omega v w d\boldsymbol{x},$$

and u_{0h} is the Lagrange interpolation $u(\mathbf{x},0)$ in space V_h. It is known (cf.,e.g. [23]) that we have the approximate properties

$$\|u - u_h\|_0 \lesssim h^2 |||u|||_{2,\Omega}, \quad \|\nabla u - \nabla u_h\|_0 \lesssim h |||u|||_{2,\Omega}. \tag{3}$$

where $|||u|||_{2,\Omega} = \|u_0\|_{H^2(\Omega)} + \|u\|_{L^\infty([0,T],H^2(\Omega))} + \|u_t\|_{L^2([0,T],H^2(\Omega))}$.

Next we present the semi-discrete finite volume element method for (1). For this purpose, we first define the so-called *dual mesh* of Ω. For $P \in \mathcal{N}_h$, let the so-called *control volume* V_P be some polygon surrounding P such that all control volumes V_P, $P \in \mathcal{N}_h$, construct another partition $\mathcal{T}_h^*$ of Ω. For instance, when $\mathcal{T}_h$ is a triangular mesh, for all $P \in \mathcal{N}_h$, the control volume V_p is a polygon surrounding P by successively connecting the midpoints of an edge in $\mathcal{E}_P = \{e \in \mathcal{E}_h : P \in \bar{e}\}$ and the barycenter of $\tau \subset \omega_P = \bigcup\{\tau' \in \mathcal{T}_h : P \in \bar{\tau}'\}$, see Figure 1 for the dual mesh $\mathcal{T}_h^*$. Associated with $\mathcal{T}_h^*$, we define a test space

$$V_h^* = \{\chi_{V_P} : P \in \mathring{\mathcal{N}}_h\},$$

where for any subset $S \subset \Omega$, the characteristic function $\chi_S = 1$ in S and $\chi_S = 0$ in $\Omega \setminus S$. Since $\dim V_h = \dim V_h^* = \#\mathring{\mathcal{N}}_h$, there exists a linear bijection $\Pi : V_h \to V_h^*$

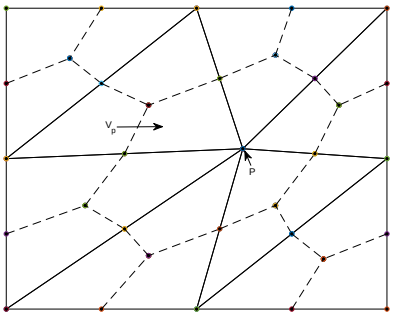

FIGURE 1. A dual mesh $\mathcal{T}_h^*$ of a triangular mesh : each control volume is a polygon surrounding P which is depicted with dotted line.

which maps $v_h = \sum_{P \in \mathcal{N}_h} v_h(P) \in V_h$ to $v_h^* = \Pi v_h = \sum_{P \in \mathcal{N}_h} v_h(P) \chi_{V_P} \in V_h^*$.

The semi-discrete finite volume scheme for (1) is to find $u_{h,v}(\cdot,t) \in V_h, t \in [0,T]$, such that

$$\begin{cases} (u_{h,v,t}(\cdot,t), v_h^*) + a_v(u_{h,v}(\cdot,t), v_h^*) = (f(\cdot,t), v_h^*), \quad \forall v_h^* \in V_h^*, \\ u_{h,v}(\mathbf{x},0) = u_{0h,v}(\mathbf{x}), \quad \mathbf{x} \in \Omega, \end{cases} \tag{4}$$

where for all $v \in H_0^1(\Omega) \cap H^2(\Omega)$,$v_h^* \in V_h^*$,

$$a_v(v, v_h^*) = -\sum_{P \in \mathcal{N}_h} \int_{\partial V_P} \kappa \nabla v \cdot \mathbf{n} v_h^* d\boldsymbol{x},$$

where $\mathbf{n}$ is the outward unit normal vector at the boundary ∂V_P. For this finite volume solution, we have the following error estimates (cf.,e.g. [17, 27])

$$\begin{aligned} &\|u - u_{h,v}\|_0 \lesssim h^2(\|u_0\|_{H^3(\Omega)} + \|u_t\|_{L^2([0,T],H^3(\Omega))}), \\ &\|\nabla u - \nabla u_{h,v}\|_0 \lesssim h|||u|||_{2,\Omega}. \end{aligned} \tag{5}$$

Let us compare these two semi-discrete schemes. On one hand, since the mass matrix $M = [(\phi_j, \phi_i)]$ and the stiffness matrix $K = [a(\phi_j, \phi_i)]$ are symmetric, there are many fast solvers (such as the conjugate gradient method (CG)) for the linear algebraic system derived from the the finite element scheme (2). While for the FVM scheme, the stiffness matrix $K_v = [a_v(\phi_j, \psi_i)]$ is usually non-symmetric, one has to seek other fast solver such as the generalized minimal residual method (GMRES) to solve the corresponding linear system. Moreover, if the exact solution of (1) is sufficiently regular, both schemes have optimal convergence order both under the H^1 and L^2 norm. However, to guarantee the optimal convergence order under the L^2 norm, the regularity-condition on the solution is often more strict for the FVM than that for the FEM. On the other hand, letting $v_h^* = \phi_P^*$ in (4), we find that $u_{h,v}$ satisfy the following semi-discrete local conservation law

$$\int_{V_P} u_{h,v,t} d\boldsymbol{x} - \int_{\partial V_P} \kappa \nabla u_{h,v} \cdot \mathbf{n} dl = \int_{V_P} f d\boldsymbol{x}, \tag{6}$$

on each control volume $V_P, P \in \mathring{\mathcal{N}}_h$. However, in general the finite element solution u_h does not satisfy the above local conservation law, namely,

$$\int_{V_P} u_{h,t} d\boldsymbol{x} - \int_{\partial V_P} \kappa \nabla u_h \cdot \mathbf{n} dl \neq \int_{V_P} f d\boldsymbol{x}, \quad \forall P \in \mathcal{N}_h.$$

Of course, by a similar argument in [32], it is not difficult to find the FEM solution satisfies the following *almost* local conservation property :

$$\sum_{P \in \mathcal{N}_h} \left| \int_{V_P} u_{h,t} d\boldsymbol{x} - \int_{\partial V_P} \kappa \nabla u_h \cdot \mathbf{n} dl - \int_{V_P} f d\boldsymbol{x} \right| \lesssim h,\ t \in (0, T]. \tag{7}$$

where the hidden constant depends only on the shape-regularity of $\mathcal{T}_h$.

In summary, both the FEM and the FVM are nice numerical schemes for (1). The FEM has some (weak) advantages in the computational speed and accuracy. The FVM has the advantage of preserving local conservation laws which are highly desired by physicists. For this reason and for the fact that the FEM solution also satisfies the *almost* local conservation property (7), one natural idea is to post-process the FEM solution so that its numerical flux satisfy the local conservation law. Note that this post-processing idea has been applied to the elliptic equations in many papers([4, 5, 7, 14, 15, 22, 28, 32]), during the past several decades. However, to the best of our knowledge, this idea has not been applied to the parabolic problems yet. The goal of the following sections of this paper is to apply this post-processing technique to parabolic problems.

We end this section by introducing two elliptic projection operators as below. Firstly, let the finite element projector $P_h : v \in H_0^1(\Omega) \to P_h v_h \in V_h$ be defined by

$$a(P_h v, v_h) = a(v, v_h),\ \forall v_h \in V_h.$$

Secondly, let the finite volume projector

$$P_h^* : v \in H^2(\Omega) \cap H_0^1(\Omega) \to P_h^* v \in V_h$$

be defined by

$$a_v(P_h^* v, v_h^*) = a_v(v, v_h^*),\ \forall v_h^* \in V_h^*.$$

Note that when $v \in H^2(\Omega)$ and $\kappa \in W^{2,\infty}(\Omega)$, we have the following superconvergence property(cf.,[26])

$$\|\nabla P_h^* v - \nabla P_h v\|_0 \lesssim h^2 \|v\|_{H^2(\Omega)}. \tag{8}$$

3. Post-processing of semi-discrete schemes

In this section, we present two approaches to post-process the semi-discrete finite element solution u_h which has been already computed by the scheme (2). This two approaches were first introduced in [32] for elliptic equations, here we apply them to parabolic problems.

3.1. Continuous locally conservative flux. The goal of this subsection is to derive a continuous flux function which satisfies the conservation law in each control volume of the dual mesh $\mathcal{T}_h^*$. Namely, we will derive a continuous flux function $\tilde{p}_h$ to approximate the the exact flux $p = p(\boldsymbol{x}, t) = -\kappa \nabla u(\boldsymbol{x}, t)$ which satisfies the conservation laws

$$\int_{V_P} u_{h,t} d\boldsymbol{x} + \int_{\partial V_P} \tilde{p}_h \cdot \mathbf{n} dl = \int_{V_P} f d\boldsymbol{x}, \quad \forall P \in \mathcal{N}_h. \tag{9}$$

To this end we post-process the existed *discrete flux* $p_h = -\kappa \nabla u_h$ which can be computed directly after the obtain of the semi-discrete finite element solution u_h. We observe that p_h is usually discontinuous across each edge of $\mathcal{T}_h$ due to the discontinuity of ∇u_h across the edge. To obtain a continuous flux, we use the popular gradient recovery technique (see e.g. [31, 20]). Let G_h: $V_h \to V_h \times V_h$ be a gradient recover operator which satisfies the boundedness

$$\|G_h v_h\|_{0,\tau} \lesssim \|\nabla v_h\|_{0,\mathcal{K}_\tau}, \quad \forall v_h \in V_h, \tag{10}$$

where $\mathcal{K}_\tau = \bigcup\{\omega_P : P \text{ is the vertex of } \tau\}$, and the approximation property

$$\|\nabla u - G_h u_h\|_{0,\Omega} \lesssim h \|u\|_{2,\Omega}, \quad \forall u \in H^2(\Omega). \tag{11}$$

Since $G_h u_h$ is continuous across each edge, $-\kappa G_h u_h$ does either. However, the flux $-\kappa G_h u_h$ does not satisfy the local conservation law (9). To derive a locally conservative flux, we update $-\kappa G_h u_h$ by adding some appropriate bubble in each triangle $\tau = \triangle P_1 P_2 P_3 \in \mathcal{T}_h$ as below. Let λ_i, $i = 1, 2, 3$, be the barycentric coordinates corresponding to the vertices P_i, $i = 1, 2, 3$. Moreover, we define the residual of u_h on the element τ as a functional valued on functions in V_h which is given for all $v_h \in V_h$ by

$$\begin{aligned} R(v_h, \tau) \quad = \quad & \int_\tau [(u_{h,t} - f)(v_h - v_h^*) - p_h \cdot \nabla v_h] d\boldsymbol{x} \\ & + \int_{\partial\tau} \kappa G_h u_h \cdot \mathbf{n} (v_h^* - v_h) dl. \end{aligned} \tag{12}$$

We are now ready to present our locally conservative flux $\tilde{p}_h$. In each $\tau \in \mathcal{T}_h$, let

$$\tilde{p}_h = -\kappa G_h u_h + \lambda_1 \lambda_2 \lambda_3 \begin{pmatrix} c_1 \\ c_2 \end{pmatrix}, \tag{13}$$

where c_1, c_2 are two parameters determined by

$$\int_{(\partial V_{P_i})\cap\tau} \tilde{p}_h \cdot \mathbf{n} dl = R(\lambda_i, \tau), i = 1, 2, 3. \tag{14}$$

Note that here, we have only two parameters but three constrains. Since

$$\sum_{i=1}^{3} R(\lambda_i, \tau) = R(\sum_{i=1}^{3} \lambda_i, \tau) = R(1, \tau) = 0$$

and

$$\sum_{i=1}^{3} \int_{(\partial V_{P_i})\cap\tau} \tilde{p}_h \cdot \mathbf{n} dl = \sum_{i=1}^{3} \int_{e_i} [\tilde{p}_h] \cdot \boldsymbol{n}_{\boldsymbol{e_i}} = 0,$$

where $e_i, i = 1, 2, 3$ are the three edges of the dual mesh $\mathcal{T}_h^*$ in τ, only two of three equations in (14) are linear independent. Namely the equations in (14) can be reduced to a 2×2 linear system. Following the same arguments in [32] on the existence and uniqueness of $\tilde{p}_h$ for elliptic equations and noting that the only difference of the linear system here from that in [32] is that f is replaced by $f - u_{h,t}$, we are easy to show that (14) admits a unique solution $\tilde{p}_h$.

On the other hand, noticing $\kappa G_h u_h$ is continuous across each edge in $\mathcal{T}_h$ and u_h is the solution of (2), we have

$$\begin{aligned}
\int_{\partial V_P} \tilde{p}_h \cdot \mathbf{n} dl &= \sum_{\tau \subset \omega_P} R(\phi_P, \tau) \\
&= \int_{\omega_P} [(f - u_{h,t})(\phi_P^* - \phi_P) - p_h \cdot \nabla \phi_P] d\boldsymbol{x} \\
&= \int_{\omega_P} (f - u_{h,t}) \phi_P^* d\boldsymbol{x} = \int_{V_P} (f - u_{h,t}) d\boldsymbol{x},
\end{aligned}$$

where for all $P \in \mathcal{N}_h$, ϕ_P is the corresponding nodal basis, $\omega_P = \text{Supp}\phi_p$ and V_P is the volume associated with the vertex P. Namely, the flux $\tilde{p}_h$ satisfies the local conservation law (9) in each V_p.

We close this subsection with a discussion on the approximation property of $\tilde{p}_h$. We claim that

$$\|\tilde{p}_h - p\|_0 \lesssim h |||u|||_{2,\Omega}. \tag{15}$$

In fact, it is easy to deduce from the definition (13) and (14) that

$$|c_j| \lesssim h^{-1} R_\tau, \ (j = 1, 2),$$

where $R\tau = \max_{1 \leqslant i \leqslant 3} |R_{i,\tau}|$, and $R_{i,\tau} = R(\lambda_i, \tau) + \int_{(\partial V_{P_i})\cap\tau} \kappa G_h u_h \cdot \mathbf{n} dl$. Then,

$$\|\tilde{p}_h - p\|_{0,\tau} \lesssim R_\tau.$$

Noticing that

$$\int_{\tau \cap V_{P_i}} (f - u_t) d\boldsymbol{x} = \int_{\tau \cap V_{P_i}} -\nabla \cdot (\kappa \nabla u) d\boldsymbol{x} = \int_{\partial(V_{P_i} \cap \tau)} p \cdot \mathbf{n} dl,$$

and

$$\int_\tau (f - u_t) \lambda_i d\boldsymbol{x} = \int_{\partial\tau} p \cdot \mathbf{n} \lambda_i dl - \int_\tau p \cdot \nabla \lambda_i d\boldsymbol{x},$$

we have

$$\begin{aligned} R_{i,\tau} &= \int_\tau [(u_{h,t}-f)\lambda_i - p_h\cdot\nabla\lambda_i]d\boldsymbol{x} - \int_{\partial\tau}\kappa G_h u_h\cdot\mathbf{n}\lambda_i dl \\ &\quad + \int_\tau (f-u_{h,t})\lambda_i^* d\boldsymbol{x} + \int_{\partial\tau}\kappa G_h u_h\cdot\mathbf{n}\lambda_i^* + \int_{(\partial V_{P_i})\cap\tau}\kappa G_h u_h\cdot\mathbf{n}dl \\ &= \int_\tau [(u_{h,t}-u_{h,v,t})\lambda_i + (p_{h,v}-p_h)\cdot\nabla\lambda_i]d\boldsymbol{x} - \int_{\partial\tau}(p_{h,v}+\kappa G_h u_h)\cdot\mathbf{n}\lambda_i dl \\ &\quad + \int_{\tau\cap V_{P_i}}(u_{h,v,t}-u_{h,t})d\boldsymbol{x} + \int_{\partial(\tau\cap V_{P_i})}(p_{h,v}+\kappa G_h u_h)\cdot\mathbf{n}dl, \end{aligned}$$

where $p_{h,v} = -\kappa\nabla u_{h,v}\cdot\mathbf{n}$ is the finite volume flux. For $t\in(0,T]$, by the trace theorem,

$$\begin{aligned} |R_\tau| \lesssim & \|u_{h,t}-u_{h,v,t}\|_{0,\tau} + \|p_{h,v}-p_h\|_{0,\tau} \\ & + \|p_{h,v}+\kappa G_h u_h\|_{0,K_\tau} + h_\tau|p_{h,v}+\kappa G_h u_h|_{1,K_\tau} \\ \lesssim & \|u_{h,t}-u_{h,v,t}\|_{0,\tau} + \|\nabla u_{h,v}-\nabla u_h\|_{0,\tau} \\ & + \|\nabla u_{h,v}-G_h u_h\|_{0,K_\tau} + h_\tau|\nabla u_v - G_h u_h|_{1,K_\tau}. \end{aligned}$$

Summing τ for all $\tau\in\mathcal{T}_h$, we obtain

$$\begin{aligned} \|p-\tilde{p}_h\|_0 \lesssim & \|u_{h,t}-u_{v,t}\|_0 + \|\nabla u_{h,v}-\nabla u_h\|_0 \\ & + \|\nabla u_{h,v}-G_h u_h\|_0 + h|\nabla u - G_h u_h|_1. \end{aligned}$$

By (3), (5), (11), the inverse inequality and the supercloseness property (8), we obtain the estimate (15).

In summary, by the post-processing techniques in this subsection, we obtain a continuous locally conservative numerical flux function which converges to the exact flux with optimal convergence order.

3.2. Finite-volume-element-like solutions. In this subsection, we post-process the finite element solution u_h to derive a function $\hat{u}_h$ which satisfies the following properties. First, $\hat{u}_h$ is globally continuous in Ω and is a polynomial in each element $\tau\in\mathcal{T}_h$. Secondly, $\hat{u}_h$ satisfies the conservation law in each control volume $V_P, P\in\mathring{\mathcal{N}}_h$. Thirdly, $\hat{u}_h$ converges to the exact solution u with optimal convergence rates both in H^1 and L^2 space. Note that the finite volume element solution $u_{h,v}$ defined in (4) also satisfies the above three properties, we call $\hat{u}_h$ a *finite-volume-element-like* solution.

Next we present our post-processing method to derive $\hat{u}_h$. For this purpose, we first enlarge the finite element space V_h to $\widehat{V}_h$ by adding bubbles defined on elements. That is, in each element $\tau=\triangle P_1P_2P_3\in\mathcal{T}_h$, we enlarge the finite element space $V_h|_\tau$ to $\widehat{V}_h|\tau$ by letting

$$\widehat{V}_h|_\tau = V_h|_\tau \oplus span\{\lambda_1^2\lambda_2\lambda_3, \lambda_1\lambda_2^2\lambda_3, \lambda_1\lambda_2\lambda_3^2\}.$$

Now we let

$$\hat{u}_h = u_h + \lambda_1\lambda_2\lambda_3\sum_{j=1}^{3}c_j(t)\lambda_j \in \widehat{V}_h, \tag{16}$$

with the three functions $c_1(t)$, $c_1(t)$ and $c_3(t)$ determined by the constrains

$$\int_{V_{P_i}\cap\tau}\hat{u}_{h,t}d\boldsymbol{x} - \int_{(\partial V_{P_i})\cap\tau}\kappa\nabla\hat{u}_h\cdot\mathbf{n}dl = S(\phi_{P_i},\tau), (i=1,2,3). \tag{17}$$

with the residual functional defined for all $v_h \in V_h$ by

$$S(v_h,\tau)=\int_\tau [u_{h,t}v_h - p_h\nabla v_h + f(v_h^*-v_h)]d\boldsymbol{x} - \int_{\partial\tau}\{p_h\}\cdot\mathbf{n}(v_h^*-v_h)dl.$$

In the above equality, $\{\cdot\}$ is an averaging operator defined on an internal edge or part of the internal edge sharing by two elements τ_1 and τ_2 for vector $\boldsymbol{v}$ as

$$\{\boldsymbol{v}\}=\frac{\boldsymbol{v}|_{\tau_1}+\boldsymbol{v}|_{\tau_2}}{2}.$$

In particular, the initial $\hat{u}_{0h}=\hat{u}_h(\cdot,0)=u_{0h}+\lambda_1\lambda_2\lambda_3\sum_{j=1}^3 c_j(0)\lambda_j \in \widehat{V}_h$ are determined by letting

$$-\int_{(\partial V_{P_i})\cap\tau}\kappa\nabla\hat{u}_{0h}\cdot\mathbf{n}dl = S_0(\phi_{P_i},\tau),\ (i=1,2,3), \tag{18}$$

where

$$S_0(v_h,\tau)=\int_{\partial\tau}\{\kappa\nabla u_{0h}\}\cdot\mathbf{n}(v_h^*-v_h)dl+\int_\tau[\nabla u_{0h}\nabla v_h+f(0)(v_h^*-v_h)]d\boldsymbol{x}.$$

The existence and uniqueness of the initial value $\hat{u}_{0h}$ has been proved in [32]. The following theorem shows the existence and uniqueness of $\hat{u}_h(\cdot,t)$ for all $t\in[0,T]$.

Theorem 3.1. *For all $t\in(0,T]$ and all $\tau\in\mathcal{T}_h$, there exists a unique $\hat{u}_h$ satisfying* (16) *and* (17).

Proof. By (17), we obtain a 3×3 linear algebra system

$$\mathbf{A}_\tau\mathbf{c}_\tau^{'}(t)+\mathbf{D}_\tau\mathbf{c}_\tau(t)=\mathbf{b}_\tau(t), \tag{19}$$

where $\mathbf{A}_\tau=(a_{ij})(i,j=1,2,3)$ with

$$a_{ij}=\int_{V_{P_i}\cap\tau}\lambda_1\lambda_2\lambda_3\lambda_j d\boldsymbol{x}, \tag{20}$$

$\mathbf{D}_\tau=(d_{ij})(i,j=1,2,3)$ with

$$d_{ij}=\int_{(\partial V_{P_i})\cap\tau}\kappa\nabla\lambda_1\lambda_2\lambda_3\lambda_j\cdot\mathbf{n}dl, \tag{21}$$

and $\mathbf{b}_\tau(t)=(b_1,b_2,b_3)^T$ with

$$b_i=S(\lambda_i,\tau)-(\int_{V_{P_i}\cap\tau}u_{h,t}d\boldsymbol{x}+\int_{(\partial V_{P_i})\cap\tau}p_h\cdot\mathbf{n}dl),(i=1,2,3). \tag{22}$$

Let $|\tau|$ be the measur of the element τ, it is easy to obtain that

$$det(\mathbf{A}_\tau)=\frac{289|\tau|^3}{18329090580},$$

which is always positive, thus matrix $\mathbf{A}_\tau$ is invertible. Then we can rewrite the linear algebra system (19) of ordinary differential equations as

$$\mathbf{c}_\tau^{'}(t)+\mathbf{A}_\tau^{-1}\mathbf{D}_\tau\mathbf{c}_\tau(t)=\mathbf{A}_\tau^{-1}\mathbf{b}_\tau(t). \tag{23}$$

From the ordinary differential equation theory we known that (23) has a unique solution with initial value $\mathbf{c}_\tau(0)$ (see e.g. [1]). This completes the proof. □

Next we verify that $\hat{u}_h$ satisfies the three aforementioned properties shared by the FVM solution $u_{h,v}$. First, it is easy to see that $\hat{u}_h$ is globally continuous and is a polynomial of degree 4 in each element $\tau \in \mathcal{T}_h$. Secondly, $\hat{u}_h$ satisfies the semi-discrete conservation law (6). In fact for all vertex $P \in \mathcal{N}_h$, by letting $v_h = \phi_P$ in (17), we have

$$\begin{aligned}\int_{V_P} \partial_t \hat{u}_h^n d\boldsymbol{x} - \int_{\partial V_P} \kappa \nabla \hat{u}_h^n \cdot \mathbf{n} dl &= \sum_{\tau \subset \omega_P} S(\phi_P, \tau) \\ &= \int_{\omega_P} [f(\phi_P^* - \phi_P) + u_{h,t}\phi_P - p_h \cdot \nabla \phi_P] d\boldsymbol{x} \\ &= \int_{\omega_P} f\phi_P^* d\boldsymbol{x} = \int_{V_P} f d\boldsymbol{x},\end{aligned}$$

where the average $\{p_h\}$ is continuous cross each edge $e \in \mathcal{E}_h$ is used in the second equality and the identity $(u_{h,t}, \phi_P) - (p_h, \nabla \phi_P) = (f, \phi_P)$ is used in the third equality. In the end, we prove that $\hat{u}_h$ converges with optimal convergence rates. Namely, we will show the following estimates.

$$\|u - \hat{u}_h\|_0 \lesssim h^2 |||u|||_{2,\Omega}, \quad \|\nabla u - \nabla \hat{u}_h\|_0 \lesssim h |||u|||_{2,\Omega}. \tag{24}$$

In fact, by (18) and (22), we have

$$\begin{aligned} b_i &= \int_\tau (u_{h,t} - u_t)(\lambda_i - \lambda_i^*) d\boldsymbol{x} + \int_\tau (p - p_h) \nabla \lambda_i d\boldsymbol{x} \\ &\quad + \int_{(\partial V_{P_i}) \cap \tau} (p - p_h) \cdot \mathbf{n} dl + \int_{\partial \tau} (p - \{p_h\}) \cdot \mathbf{n} (\lambda_i^* - \lambda_i) dl, \end{aligned}$$

then for $t \in (0, T]$,

$$|b_i| \lesssim \|u_{h,t} - u_t\|_{0,\tau} + \|\nabla u - \nabla u_h\|_{0,\tau} + h_\tau |\nabla u - \nabla u_h|_{1,\tau} \, (i = 1, 2, 3).$$

On the other hand, noting that $\mathbf{A}_\tau^{-1}$ and $\mathbf{D}_\tau$ is independent of time variable t, $\mathcal{T}_h$ is a quasi-uniform and shape-regular partition and κ is uniformly bounded, thus $\mathbf{A}_\tau^{-1}$ and $\mathbf{D}_\tau$ are uniformly bounded. That is, $\|\mathbf{A}_\tau^{-1}\|_0 \lesssim 1$ and $\|\mathbf{D}_\tau\|_0 \lesssim 1$. Therefore, we obtain that for $t \in (0, T]$,

$$|c_i| \lesssim \|u_{h,t} - u_t\|_{0,\tau} + \|\nabla u - \nabla u_h\|_{0,\tau} + h_\tau |\nabla u - \nabla u_h|_{1,\tau} \, (i = 1, 2, 3).$$

Consequently, by the triangle inequality and the error estimates (3), we obtain (24).

4. Post-processing of fully-discrete schemes.

In this section, we implement the two aforementioned post-processing approaches by taking the *backward Euler* scheme as an example of temporal discretization. Let Δt be the time step size and $t_n = n\Delta t, n = 0, 1, 2, \dots$, be the time levels. The fully-discrete FEM solution $u_h^n \in V_h$, which is an approximations of $u(\cdot, t_n)$, satisfies following backward Euler-finite element scheme

$$\begin{cases} (\bar{\partial}_t u_h^n, v_h) + a(u_h^n, v_h) = (f(\cdot, t_n), v_h), \quad \forall v_h \in V_h, \\ u_h(\mathbf{x}, 0) = u_{0h}(\mathbf{x}), \quad \mathbf{x} \in \Omega, \end{cases} \tag{25}$$

where $\bar{\partial}_t u_h^n = (u_h^n - u_h^{n-1})/\Delta t$ is the backward Euler difference operator. Similarly, the backward Euler-finite volume element scheme is to find solution $u_{h,v}^n \in V_h$ such that

$$\begin{cases} (\bar{\partial}_t u_{h,v}^n, v_h^*) + a_v(u_{h,v}^n, v_h^*) = (f(\cdot, t_n), v_h^*), \quad \forall v_h^* \in V_h^*, \\ u_{h,v}(\mathbf{x}, 0) = u_{0h}(\mathbf{x}), \quad \mathbf{x} \in \Omega. \end{cases} \tag{26}$$

Then we introduce the fully discrete conservation law: find a pair $(U_P^n; \mathcal{F}_P^n)$ to approximate the average value of $u(\cdot, t_n)$ and the average flux over the control volume V_P, such that

$$\frac{U_P^n - U_P^{n-1}}{\Delta t} + \mathcal{F}_P^n = F_P^n, \quad \forall P \in \mathcal{N}_h, \tag{27}$$

where

$$F_P^n = \frac{1}{|V_P|} \int_{V_P} f(\cdot, t_n) d\boldsymbol{x} \tag{28}$$

is the average value of $f(\cdot, t_n)$ over the control volume V_P. Notice that if we choose $v_h^* = \chi_{V_P}$ in (26) and then dividing by $|V_P|$, the measure of V_P, we find that the pair $(U_{P_v}^n; \mathcal{F}_{P_v}^n)$ obtained from the FVM solution $u_{h,v}^n$ satisfies the discrete conservation law (27), where

$$U_{P_v}^n = \frac{1}{|V_P|} \int_{V_P} u_{h,v}^n d\boldsymbol{x}, \tag{29}$$

and

$$\mathcal{F}_{P_v}^n = -\frac{1}{|V_P|} \int_{\partial V_P} \kappa \nabla u_{h,v}^n \cdot \mathbf{n} dl. \tag{30}$$

However, similarly, the pair $(U_P^n; \mathcal{F}_P^n)$ obtained from the FEM solution u_h^n does not satisfy the conservation law (27), so we want to post-process it.

Next we explain how to implement the two post-processing techniques in the previous section. This can be reduced to solving linear system (14) and (17). Then we will discuss how to solve these two linear systems respectively. First, applying the post-processing technique presented in subsection 3.1, we only need to modify the average flux $\mathcal{F}_P^n = \frac{1}{|V_P|} \int_{\partial V_P} p_h^n \cdot \mathbf{n} dl$ to $\widetilde{\mathcal{F}}_P^n = \frac{1}{|V_P|} \int_{\partial V_P} \tilde{p}_h^n \cdot \mathbf{n} dl$ such that $(U_P^n; \widetilde{\mathcal{F}}_P^n)$ satisfies (27). That is, at $t = t_n$, we post-process u_h^n to construct a continuous flux

$$\tilde{p}_h^n = -\kappa G_h u_h^n + \lambda_1 \lambda_2 \lambda_3 \begin{pmatrix} c_1^n \\ c_2^n \end{pmatrix}, \tag{31}$$

where c_1^n and c_2^n are constants to be determined, such that satisfies

$$\int_{(\partial V_{P_i}) \cap \tau} \tilde{p}_h^n \cdot \mathbf{n} dl = \bar{R}(\tau, \lambda_i), (i = 1, 2, 3), \tag{32}$$

where

$$\bar{R}(\tau, \lambda_i) = \int_\tau [(\bar{\partial}_t u_h^n - f(\boldsymbol{x}, t_n))(\lambda_i - \lambda_i^*) - p_h^n \nabla \lambda_i] d\boldsymbol{x}. \tag{33}$$

In (33), we have replaced the differential operator in (12) with the difference operator. Let (x_i, y_i) be the coordinates of P_i and let $x_{i+3} = x_i$, $y_{i+3} = y_i$, $i = 1, 2, 3$. Then we derive the following linear system from (32),

$$\begin{pmatrix} y_1 - y_2 & x_2 - x_1 \\ y_3 - y_2 & x_2 - x_3 \end{pmatrix} \begin{pmatrix} c_1^n \\ c_2^n \end{pmatrix} = \frac{864}{11} \begin{pmatrix} RHS_1 \\ RHS_2 \end{pmatrix}, \tag{34}$$

where $RHS_j = \bar{R}(\tau, \lambda_j) + \int_{\partial \tau} \kappa G_h u_h^n \cdot \mathbf{n} dl, j = 1, 2$. Since P_1, P_2 and P_3 are three different vertices of $\tau = \triangle P_1 P_2 P_3$, linear system (34) admits a unique solution. Noting that the coefficient matrix of (34) is time independent, so we can calculate it independently and only once. After these preparations, the implementation process can be summarized as the following algorithm.

Algorithm 4.1. *Suppose u_h^n has computed by the scheme* (25)*, we design the continuous local-conserving flux by the following steps.*

Step 1. *Compute the continuous gradient* $G_h u_h^n$ *by the gradient recovery technique.*
Step 2. *For all* $\tau \in \mathcal{T}_h$*, compute the coefficient matrix of* (34).
Step 3. *For all* $\tau \in \mathcal{T}_h$ *and for all* $t = t_n$*, compute* RHS_1 *and* RHS_2 *in* (34).
Step 4. *Solve the linear system* (34).
Step 5. *Calculate* $\hat{p}_h^n$ *by* (31).

Since the time accuracy of the backward Euler scheme is $O(\Delta t)$, $\tilde{p}_h^n$ satisfies the following convergence property

$$\|p(\cdot, t_n) - \tilde{p}_h^n\|_0 \lesssim \Delta t + h. \tag{35}$$

We note that the implementation of Algorithm 4.1 does not depend on time levels or element numbers, so we can compute in parallel for both time levels and elements. In summary, the implementation of Algorithm 4.1 only needs to solve a 2×2 linear system in each element and can be embedded into the existing finite element solver. And Algorithm 4.1 can be implemented in parallel on a mainframe computer with very little computation time.

Then to implement the post-processing technique presented in subsection 3.2, we post-process u_h^n to $\hat{u}_h^n$ such that the associated $(\widehat{U}_P^n; \widehat{\mathcal{F}}_P^n)$ satisfies (27). That is, we will show how to solve the ordinary differential equations (23). After time discretization, this can be reduced to solve the discrete form of (23). In details, in each element, we construct the finite-volume-element-like solution

$$\hat{u}_h^n = u_h^n + \lambda_1\lambda_2\lambda_3 \sum_{j=1}^{3} c_j^n \lambda_j, \tag{36}$$

where c_1^n, c_2^n and c_3^n are constants satisfiying

$$\int_{V_{P_i} \cap \tau} \bar{\partial}_t \hat{u}_h^n d\boldsymbol{x} - \int_{(\partial V_{P_i}) \cap \tau} \kappa \nabla \hat{u}_h^n \cdot \mathbf{n} dl = \bar{S}(\tau, \lambda_i), \tag{37}$$

where

$$\bar{S}(\tau, \lambda_i) = \int_\tau [\bar{\partial}_t u_h^n \lambda_i - p_h^n \nabla \lambda_i + f(t_n)(\lambda_i^* - \lambda_i)] d\boldsymbol{x} - \int_{\partial\tau} \{p_h^n\} \cdot \mathbf{n} (\lambda_i^* - \lambda_i) dl.$$

From (37), we obtain the discrete form of (23)

$$(\mathbf{A}_\tau + \Delta t \mathbf{D}_\tau)\mathbf{c}_\tau^n = \Delta t \mathbf{b}_\tau^n + \mathbf{A}_\tau \mathbf{c}_\tau^{n-1}, \tag{38}$$

where $\mathbf{c}_\tau^n = (c_1^n, c_2^n, c_3^n)^T$ and $\mathbf{b}_\tau^n = (b_1^n, b_2^n, b_3^n)^T$ with

$$b_i^n = \bar{S}(\tau, \lambda_i) - (\int_{V_{P_i} \cap \tau} \bar{\partial}_t u_h^n d\boldsymbol{x} + \int_{(\partial V_{P_i}) \cap \tau} p_h^n \cdot \mathbf{n} dl), i = 1, 2, 3.$$

It can be seen from (20) that $\mathbf{A}_\tau$ is a positive definite matrix, thus the eigenvalues of $\mathbf{A}_\tau$ are positive. When the time step Δt is small enough, the eigenvalues of $\mathbf{A}_\tau + \Delta t \mathbf{D}_\tau$ are also positive. Therefore the coefficient matrix of (38) is positive definite and the linear system (38) admits a unique solution. From (20) and (21), we note that the matrix $\mathbf{A}_\tau$ and $\Delta t \mathbf{D}_\tau$ are independent of time levels, so we only need to calculate the coefficient matrix of (38) once.

The post-processing process can be summarize by the following algorithm.

Algorithm 4.2. *Suppose* u_h^n *has computed by the scheme* (25)*, we design the finite-volume-element-like solution by the following steps.*

Step 1. *At* $t = 0$*, compute the initial value* $\mathbf{c}_\tau(0)$ *by* (18).
Step 2. *For all* $\tau \in \mathcal{T}_h$*, compute the coefficient matrix of* (38).
Step 3. *At* $t = t_n$*, for all* $\tau \in \mathcal{T}_h$*, compute the vector* $\mathbf{b}_\tau^n$.

Step 4. *Solve the linear system* (38).
Step 5. *Calculate* $\hat{u}_h^n$ *by* (36).

Notice that, in Algorithm 4.2, at $t = t_n$, we only need to solve a 3×3 linear system in each element. We also note that the linear system (38) of each element are independent of each other, so we can solve them in parallel to save computing time, which is similar to Algorithm 4.1. Thus both Algorithm 4.1 and 4.2 can be implemented in a parallel environment and require very little computation cost. And the computation complex of Algorithm 4.1 and 4.2 is proportional to the time steps and the number of elements.

To close this section, we would also like to mention that our parallel programs do not depend on the discrete scheme selection. Algorithm 4.1 and 4.2 can be easily extended to other fully-discrete schemes. For example, Crank-Nicolson scheme, we only need to replace $\mathcal{F}_P^n$ and F_P^n in (27) by $(\mathcal{F}_P^n + \mathcal{F}_P^{n-1})/2$ and $(F_P^n + F_P^{n-1})/2$, respectively. That is, we post-process the Crank-Nicolson FEM solution such that satisfies the following conservation law

$$\frac{U_P^n - U_P^{n-1}}{\Delta t} + \frac{\mathcal{F}_P^n + \mathcal{F}_P^{n-1}}{2} = \frac{F_P^n + F_P^{n-1}}{2}, \quad \forall P \in \mathring{\mathcal{N}}_h. \tag{39}$$

Since the time accuracy of the Crank-Nicolson scheme is $O(\Delta t^2)$, the corresponding conservative flux $\hat{p}_h^n$ satisfies the following convergence propery

$$\|p(\cdot, t_n) - \hat{p}_h^n\|_0 \lesssim \Delta t^2 + h. \tag{40}$$

5. Numerical Experiments

In the section, we will demonstrate the efficiency of our post-processing approaches proposed in Section 4 with a problem. Here we consider (1) with $\Omega = [0,1] \times [0,1]$, $\kappa(\boldsymbol{x}) = x_1 + x_2 + 1$ and

$$\begin{aligned} f = e^{(-log2)t}\{&[2\pi^2(x_1 + x_2 + 1) - log2]\sin \pi x_1 \sin \pi x_2 \\ &-\pi(\cos \pi x_1 \sin \pi x_2 + \sin \pi x_1 \cos \pi x_2)\}, \end{aligned}$$

which admits an exact solution $u = e^{(-log2)t} \sin \pi x_1 \sin \pi x_2$. The domain Ω is uniformly divided by triangles.

To present the experimental results, we introduce the following notations:

$$L_{u_h}^2 = \|u(\cdot, t_n) - u_h^n\|_0, \quad H_{u_h}^1 = \|u(\cdot, t_n) - u_h^n\|_1,$$

to represent errors of u_h^n under L^2 norm and H^1 norm, respectively.

First, we implement Algorithm 4.1. In this case, we choose $\Delta t = h^2$ and $T = 1$ is the final time. In fact, we can take a larger time step. And we choose such a small time step is to make sure that time errors do not affect convergence orders of spatial errors. In the Table 1, we list the errors and convergence orders of ∇u_h^n, $G_h u_h^n$ and $\tilde{p}_h^n$ under L^2 norm, respectively. In the seventh column of Table 1, we find that the convergence order of $L_{\tilde{p}_h}^2$ is 1, which confirms (35) in the theory.

Secondly, we implement Algorithm 4.2. In this case, we choose $\Delta t = 0.05h^2$ and $T = 0.1$ is the final time. We first compare the errors of the post-processed finite-volume-element-like solution with the FEM solution. From the numerical results presented in the Table 2, we find that both the errors under L^2 norm and H^1 norm of the post-processed finite-volume-element-like solution are comparable to the finite element solution's and both have optimal convergence rates.

Then we verify that the post-processed finite-volume-element-like solution satisfies conservation law (27) and the finite element solution satisfies the almost local

TABLE 1. Numerical results of Algorithm 4.1.

$1/h$	$L^2_{\nabla u_h}$	$Order$	$L^2_{G_h u_h}$	$Order$	$L^2_{\tilde{p}_h}$	$Order$
2	0.8932		0.8725		1.2090	
4	0.4401	1.02	0.3813	1.19	0.5704	1.08
8	0.2188	1.01	0.1083	1.82	0.2015	1.50
16	0.1091	1.00	0.0276	1.97	0.0844	1.26
32	0.0545	1.00	0.0069	2.00	0.0400	1.08
64	0.0273	1.00	0.0017	2.02	0.0197	1.02
128	0.0136	1.01	4.26e-4	2.00	0.0098	1.01

TABLE 2. Numerical results of Algorithm 4.2.

$1/h$	$L^2_{u_h}$	$Order$	$L^2_{\hat{u}_h}$	$Order$	$H^1_{u_h}$	$Order$	$H^1_{\hat{u}_h}$	$Order$
2	0.2182		0.2160		1.5192		1.5279	
4	0.0642	1.77	0.0640	1.75	0.8375	0.86	0.8475	0.85
8	0.0167	1.94	0.0167	1.94	0.4295	0.96	0.4309	0.98
16	0.0042	1.99	0.0042	1.99	0.2161	0.99	0.2163	0.99
32	0.0011	1.93	0.0011	1.93	0.1082	1.00	0.1083	1.00
64	2.65e-4	2.05	2.65e-4	2.05	0.0541	1.00	0.0541	1.00
128	6.54e-5	2.02	6.54e-5	2.02	0.0271	1.00	0.0271	1.00

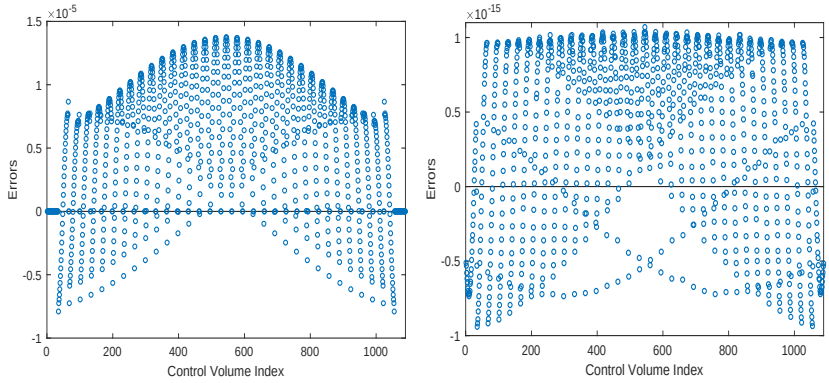

(a) (b)

FIGURE 2. Errors of conservation law: Figure 2(a) is corresponding to the FEM solution, Figure 2(b) is corresponding to the post-processed finite-volume-element-like solution.

conservation property (7). For the control volume V_P, the error of conservation law is defined as

$$E_{V_P}(w_h^n) \quad = \quad \int_{V_P} f(t_n) d\boldsymbol{x} - \int_{V_P} \bar{\partial}_t w_h^n d\boldsymbol{x} + \int_{\partial_{V_P}} \kappa \nabla w_h^n \cdot \boldsymbol{n} dl, \quad w_h^n \in V_h,$$

the summation of these errors is

$$E_S(w_h^n) = \sum_{P \in \mathring{\mathcal{N}}_h} |E_{V_P}(w_h^n)|.$$

The Figure 2(a) and 2(b) show errors of conservation law of the FEM solution and the post-processed finite-volume-element-like solution, respectively. The Figure 3 depict the summation of errors of conservation law of the FEM solution. The corresponding mesh size is $h = 1/32$. We note that local conservation errors of the FEM solution are generally not 0. And the summation of these errors converges with order 1.80, which is much better than the order 1 in theory. The order of magnitude of the local conservation error of the post-processed solution is 10^{-15}, very close to 0, which can be attributed to the errors of numerical integrations and machine accuracy. Therefore, the error of conservation law of the post-processed finite-volume-element-like solution can be view as 0 and the post-processed finite-volume-element-like solution dose satisfy local conservation law.

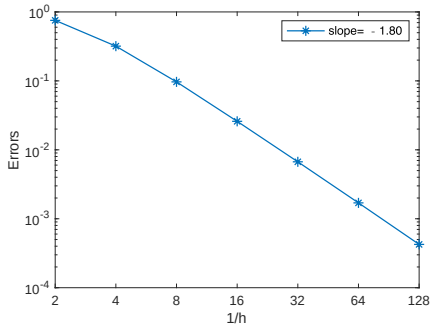

FIGURE 3. Summation of errors of conservation law.

Thirdly, we post-process the Crank-Nicolson FEM solution u_h^n to derive the global continuous flux satisfying the conservation law (39). Due to the Crank-Nicolson scheme has 2-order time accuracy, we choose $\Delta t = 0.1h$. The final time is $T = 1$. From the numerical results presented in Table 3, we find that the convergence order of $L^2_{\tilde{p}_h}$ is 1, which is also consistent with (40) in the theory.

TABLE 3. Numerical results of global continuous fluxes for post-processing Crank-Nicolson FEM solutions.

$1/h$	$L^2_{\nabla u_h}$	$Order$	$L^2_{G_h u_h}$	$Order$	$L^2_{\tilde{p}_h}$	$Order$
2	0.7779		0.7667		1.2896	
4	0.4268	0.87	0.3847	0.99	0.7071	0.87
8	0.2179	0.97	0.1148	1.74	0.2698	1.39
16	0.1093	1.00	0.0304	1.92	0.1178	1.20
32	0.0546	1.00	0.0082	1.89	0.0565	1.06
64	0.0273	1.00	0.0023	1.83	0.0279	1.02
128	0.0136	1.01	6.23e-4	1.91	0.0139	1.01

From the numerical results presented in the figures and the tables above, we have verified the theoretical results in the previous sections numerically.

6. Concluding remarks

We extend two kinds of post-processing techniques to parabolic equations to derive globally continuous flux fields and finite-volume-element-like solutions. The

post-processing is performed by adding appropriate bubble functions to the post-processed PPR-type gradient or the FEM solution. The procedures are independently on each element and so it can be calculated in parallel. Through these post-processing procedures, the derived flux fields and the finite-volume-element-like solutions both satisfy the local conservation law and have optimal convergence rates. The techniques presented here provid a better option to produce local conservation flux with high accuracy and small computational cost.

In future, we expect to extend our post-processing techniques to other types of dual mesh, such as primal meshes and nested dual meshes, and to other problems such as 3-dimensional parabolic equations.

Acknowledgments

The research was supported in part by the special project High Performance Computing of National Key Research and Development Program 2016YFB0200604, NSFC Grant 11571384, Guangdong Provincial NSF Grant 2017B030311001.

References

[1] V. I. Arnol'd. Ordinary Differential Equations. Springer-Verlag, 1992.
[2] R. E. Bank and D. J. Rose. Some error estimates for the box method. SIAM Journal on Numerical Analysis, 24(4), 777-787, 1987.
[3] T.Barth and M.Ohlberger, Finite volume methods: foundation and analysis, in Encyclopedia of Computational Mechanics, Vol. 1, John Wiley & Sons, Chichester, England, 439-474, 2004.
[4] R. Becker, D. Capatina and R. Luce. Local flux reconstructions for standard finite element methods on triangular meshes. SIAM Journal on Numerical Analysis, 54(4), 2684-2706, 2016.
[5] P. B. Bochev and M. D. Gunzburger. A locally conservative least-squares method for Darcy flows. Communications in Numerical Methods in Engineering, 24(2), 97-110, 2008.
[6] L. Chen and Y. Chen. Two-Grid method for nonlinear parabolic equations by mixed finite element methods. Journal of Scientific Computing, 49(3), 383-401, 2011.
[7] S. H. Chou and S. Tang. Conservative P1 conforming and nonconforming Galerkin FEMS: effective flux evaluation via a nonmixed method approach. SIAM Journal on Numerical Analysis, 38(2), 660-680, 2000.
[8] B. Cockburn, J. Gopalakrishnan and H. Wang. Locally conservative fluxes for the continuous Galerkin method. SIAM Journal on Numerical Analysis, 45(4), 1742-1776, 2007.
[9] J. J. Douglas, T. Dupont and M. F. Wheeler. A Galerkin procedure for approximating the flux on the boundary for elliptic and parabolic boundary value problems. Rev.franaise Automat.informat.recherche Opérationnelle Sér.rouge, 8(R-2), 22, 1974.
[10] J. Douglas, R. E. Ewing and M. F. Wheeler. The approximation of the pressure by a mixed method in the simulation of miscible displacement. RAIRO. Analyse numérique, 17(1), 17-33, 1983.
[11] Ph. Emonot. Methods de volums elements finis: applications aux equations de navier-stokes et resultats de convergence. Lyon, 1992.
[12] R. Ewing, T. Lin, and Y. Lin. On the accuracy of the finite volume element based on piecewise linear polynomials. SIAM Journal on Numerical Analysis, 39(6), 1865-1888, 2002.
[13] R.Eymard,T.Gallouet,and R.Herbin. Finite volume methods. Handbook of Numerical Analysis VII, North-Holland, Amsterdam, 713-1020, 2000.
[14] T. J. R. Hughes, G. Engel, L. Mazzei, and M. G. Larson. The continuous Galerkin method is locally conservative. Journal of Computational Physics 163, 467-488, 2000.
[15] M. G. Larson and A. J. Niklasson. A conservative flux for the continuous Galerkin method based on discontinuous enrichment. Calcolo, 41(2), 65-76, 2004.
[16] R. J. Leveque. Finite Volume Methods for Hyperbolic Problems. Cambridge University Press, Cambridge, UK, 2002.
[17] R. Li, Z. Chen and W. Wu. Generalized Difference Methods for Differential Equations: numerical analysis of finite volume methods. CRC Press, 2000.
[18] Y. Lin, M. Yang and Q. Zou. L^2 error estimates for a class of any order finite volume schemes over quadrilateral meshes. SIAM Journal on Numerical Analysis, 53(4), 2030-2050, 2015.
[19] J. D. Murray. Mathematical Biology, 2nd edn. Springer, New York (1993).

[20] A. Naga and Z. Zhang. The polynomial-preserving recovery for higher order finite element methods in 2D and 3D. Discrete and Continuous Dynamical Systems Series B, 5(3), 769-798, 2005.
[21] B. Pouliot, M. Fortin, A. Fortin and É. Chamberland. On a new edge-based gradient recovery technique. International Journal for Numerical Methods in Engineering, 93(1), 52-65, 2013.
[22] S. Sun and J. Liu. A locally conservative finite element method based on piecewise constant enrichment of the continuous Galerkin method. SIAM Journal on Scientific Computing, 31(4), 2528-2548, 2009.
[23] V. Thomée. Galerkin finite element methods for parabolic problems. Berlin: Springer-Verlag, 1984.
[24] E. Toro. Riemann Solvers and Numerical Methods for Fluid Dynamics: A Practical Introduction. Springer, Berlin, Heidelberg.
[25] X. Wang and Y. Li. L^2 error estimates for high order finite volume methods on triangular meshes. SIAM Journal on Numerical Analysis, 54(5), 2729-2749,2016.
[26] J. Xu and Q. Zou. Analysis of linear and quadratic simplicial finite volume methods for elliptic equations. Numerische Mathematik, 111(3), 469-492, 2009.
[27] M. Yang, J. Liu and Q. Zou. Unified analysis of higher-order finite volume methods for parabolic problems on quadrilateral meshes. IMA Journal of Numerical Analysis, 36(2), 872-896, 2016.
[28] S. Zhang, Z. Zhang and Q. Zou. A postprocessed flux conserving finite element solution. Numerical Methods for Partial Differential Equations, 33(6), 1859-1883, 2017.
[29] Z. Zhang and Q. Zou. Vertex-centered finite volume schemes of any order over quadrilateral meshes for elliptic boundary value problems. Numerische Mathematik, 130(2), 363-393, 2015.
[30] J. Zhu, Y. T. Zhang, A. N. Stuart and A. Mark. Application of discontinuous Galerkin methods for reaction diffusion systems in developmental biology. Journal of Scientific Computing, 40, 391-418, 2009.
[31] O. C. Zienkiewicz and J. Z. Zhu. The superconvergent patch recovery and a posteriori error estimates. Part 1: The recovery technique. International Journal for Numerical Methods in Engineering, 33(7), 1331-1364, 1992.
[32] Q. Zou, L. Guo and Q. Deng. High order continuous local-conserving fluxes and finite-volume-element-like finite element solutions for elliptic equations. SIAM Journal on Numerical Analysis, 55(6), 2666-2686, 2017.

School of Data and Computer Science, Sun Yat-sen University, Guangzhou, 510006, P.R. China.
E-mail: gongwb@mail2.sysu.edu.cn

Corresponding author. School of Data and Computer Science, Guangdong Province Key Laboratory of Computational Science, Sun Yat-sen University, Guangzhou, 510006, P.R. China.
E-mail: mcszqs@mail.sysu.edu.cn